Advances in Concrete Construction, *Vol. 9, No. 5 (2020) 511-527*
DOI: https://doi.org/10.12989/acc.2020.9.5.511

Flexural strengthening of RC one way solid slab with Strain Hardening Cementitious Composites (SHCC)

Ali Basha, Sabry Fayed and Walid Mansour*

Civil Engineering Department, Faculty of Engineering, Kafrelsheikh University, Box 33511, Kafrelsheikh, Egypt

(*Received September 25, 2019, Revised April 18, 2020, Accepted May 9, 2020*)

Abstract. The main aim of the current research is to investigate the flexural behavior of the reinforced concrete (RC) slabs strengthened with strain hardening cementitious composites (SHCC) experimentally and numerically. Seven RC slabs were prepared and tested under four-points loading test. One un-strengthened slab considered as control specimen while six RC slabs were strengthened with reinforced SHCC layers. The SHCC layers had different reinforcement ratios and different thicknesses. The results showed that the proposed strengthening techniques significantly increased the ultimate failure load and the ductility index up to 25% and 22%, respectively, compared to the control RC slab. Moreover, a three dimensional (3D) finite element model was proposed to analyze the strengthened RC slabs. It was found that the results of the proposed numerical model well agreed with the experimental responses. The validated numerical model used to study many parameters of the SHCC layer such as the reinforcement ratios and the different thicknesses. In addition, steel connectors were suggested to adjoin the concrete/SHCC interface to enhance the flexural performance of the strengthened RC slabs. It was noticed that using the SHCC layer with thickness over 40 mm changed the failure mode from the concrete cover separation to the SHCC layer debonding. Also, the steel connectors prevented the debonding failure pattern and enhanced both the ultimate failure load and the ductility index. Furthermore, a theoretical equation was proposed to predict the ultimate load of the tested RC slabs. The theoretical and experimental ultimate loads are seen to be in fairly good agreement.

Keywords: reinforced concrete; one way slab; strengthening; SHCC; ductility; finite element analysis; theoretical analysis

1. Introduction

RC elements were constructed to perform their functions proficiently over their service life. Despite that, most structures need to rehabilitation and strengthening over the design service life due to the deterioration of the structure members output from change of usage, change of the loading conditions, the lack of maintenance, the material defect and the upgrading to current design codes provisions (Sakr *et al*. 2019). Recently, numerous materials and methods for strengthening of RC structure had been developed such as the fiber reinforced polymer (FRP) and the ultra-high performance fiber reinforced concrete (UHPFRC) (Al-Osta *et al*. 2017).

Nowadays, research studies focused on strengthening RC structures using ultra high performance strain hardening cementitious composites (UHP-SHCC) (Basha *et al*. 2019). The UHP-SHCC can be easily defined as cement based matrix containing short fibers with higher mechanical properties and durability (Kunieda *et al*. 2014). Various studies reported the behavior of RC beams strengthened with UHP-SHCC layers (Khalil *et al*. 2017, Hussein *et al*. 2012, Shin *et al*. 2007, Martinola *et al*. 2010, and Qi *et al*. 2019). It was concluded that the strengthening layer improved the strength, durability, and toughness of the strengthened RC beams. Also, using the additional reinforcement embedded in the strengthening layer delayed the observed early strain localization and changed the brittle failure mode to be more ductile. Moreover, the UHP-SHCC enhanced the structural behavior of the RC slab-column connections (Cheng and Montesinos 2010, Choi *et al*. 2007, Afefy and El-Tony 2019, and Ganesan *et al*. 2015).

Although having the superior mechanical properties, the UHP-SHCC was not widely adopted in the strengthening of the RC slabs until now. Few studies were available in the literature regarding the behavior of such structures. Yun *et al*. (2010) replaced the cover at the tensile side of the RC one-way slabs with SHCC to improve the ultimate load and the ductility of RC slabs. It was shown that the use of SHCC cover had significantly increased the initial crack load, the yield load, and the ultimate load of the tested RC slabs. Also, a considerable reduction was observed in the width and the spacing of the cracks for slabs with the SHCC cover compared to the conventional RC slabs. The difference of the current research was the use of the reinforced SHCC layers with different reinforcement ratios and different thicknesses to strengthen RC slabs at its soffit.

Abbaszadeh *et al*. (2017) studied the possibility of using high performance fiber reinforced cementitious composites (HPFRCC) for retrofitting two-way RC slabs. The results showed that the proposed strengthening technique had a great effect in improving the overall structural behavior of the strengthened slabs since it achieved higher values of the

*Corresponding author, Ph.D.
E-mail: waled_mansour@eng.kfs.edu.eg

http://www.techno-press.org/?journal=acc&subpage=7
ISSN: 2287-5301 (Print), 2287-531X (Online)

Table 1The mix proportions of NSC and SHCC (kg/m3)

Material	Water content	Portland cement	Silica fume	sand	dolomite	Super plasticizer	PE fiber (12mm)	Air avoids
SHCC	292	1243	223	149	-	14.9	14.6	0.6 kg/100 kg cement
NSC	175	350	-	637	1295	-	-	-

Table 2 The mechanical properties of the concrete for both NC and SHCC

Material	Compressive strength, σ_{cu} (MPa)	Splitting tensile strength, σ_{t0} (MPa)	Flexural strength (MPa)
SHCC	47	3.50	6.50
NSC	31	3.05	4.40

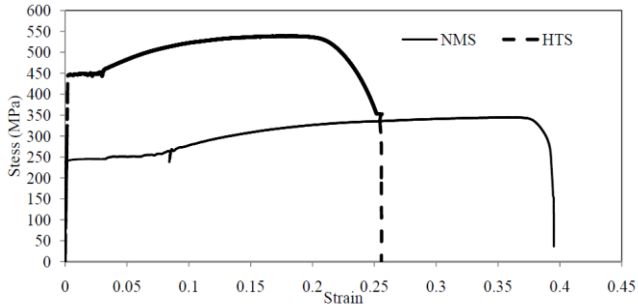

Fig. 1 Stress strain curves of reinforcing steel bars

toughness, the initial stiffness and the ductility compared to those of the control slab. Also, Radik *et al*. (2011) compared between the strengthening two-way RC floor slabs using glass-fiber-reinforced polymer (GFRP) sheets and the fiber-reinforced cement (FRC) layers. The FRC-strengthened slabs exhibited a superior ductility more than the GFRP-strengthened slabs.

Despite the valuable previous studies that investigated the behavior of RC slabs strengthened with SHCC layers, very few publications were available in the literature that discussed the flexural strengthening of RC slabs using reinforced SHCC layers with different thicknesses. In this paper, the flexural behavior of RC slabs strengthened with reinforced SHCC layers was experimentally investigated. Additionally, a numerical finite element model was proposed and verified against the experimental program. The validated numerical model was used to investigate the effect of various parameters on the behavior of the strengthened RC slabs that not included in the experimental program. Moreover, a theoretical equation was constructed to estimate the ultimate load of the strengthened RC slabs.

2. Experimental program

Six normal strength RC one way solid slabs were prepared and strengthened in the flexure with the reinforced SHCC layers in addition to a reference specimen (not strengthened). The experimental program considered the thickness and the reinforcement ratio of the SHCC layer. The flexural characteristics of the strengthened slabs will be dramatically affected with the studied parameters. Consequently, behavior of the strengthened RC slabs was compared to the result of the reference slab on the level of failure pattern, cracking load, failure load, and ductility.

2.1 Material properties

Table 1 summarized the mix proportions of the normal strength concrete (NSC) and the UHP-SHCC. The SHCC mixture was distinguished by containing silica fume to improve the density and the fluidity, the super plasticizer to secure the workability, the Polyethylene (PE) fiber to ensure the ductile behavior in addition to control propagation of the cracks, and the air avoids additives to decrease the shrinkage by increasing the mix volume. The shrinkage was resulted from the presence of high amount of cement in the mixture. The PE fibers were 0.012 mm in diameter and 12 mm in length while its weight in the mix was 1.17% of the cement weight.

To estimate the splitting tensile strength for both the NSC and the UHP-SHCC, three cylinders of 150 mm in diameter and 300 mm in height for each material were cast and tested. In the same way, three prisms had dimensions of 80×80×400 mm were prepared and tested to find the flexural strength. In addition, the compressive strength of the NSC and the SHCC were obtained by casting and testing three cubes of 150×150×150 mm for each material. The mechanical properties of the NSC and the SHCC were listed in Table 2.

The uniaxial tensile tests were performed on the reinforcing steel bars by using the universal testing machine in order to obtain its mechanical properties. The types of the used steel rebars were high tensile steel (HTS) and normal mild steel (NMS). The yield stress of the HTS and the NMS were 410 MPa and 245 MPa, respectively. The elasticity modulus of the two steel types was 200 GPa. The stress strain curves of the steel reinforcement used in the experimental investigation for both HTS and NMS were depicted in Fig. 1.

2.2 pecimen description

Seven half-scale RC slabs were prepared. One un-strengthened RC slab to represent the control specimen (S0) was casted in addition to six RC slabs were strengthened using SHCC with different strengthening schemes. Details of the slabs before the strengthening process were shown in Fig. 2. The RC slabs had the same cross-sectional dimensions of 400 mm in width, 80 mm in depth and 1800 mm in length. The loaded span of all slabs was 1700 mm. Moreover, the width of the RC slabs was reinforced by uniformly distributed bottom longitudinal reinforcement of 4D10 while the length reinforced by distributed bars of D10 mm spaced at 220 mm. The RC slabs were designed according to the Egyptian code of practice, the ECP 203-2017.

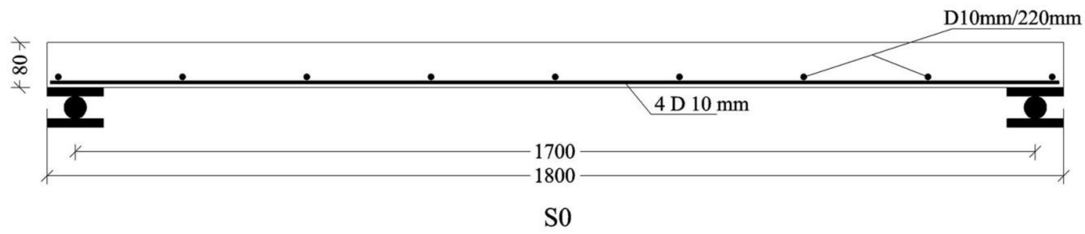

Fig. 2 Geometry and reinforcement details of the RC slabs before the strengthening process

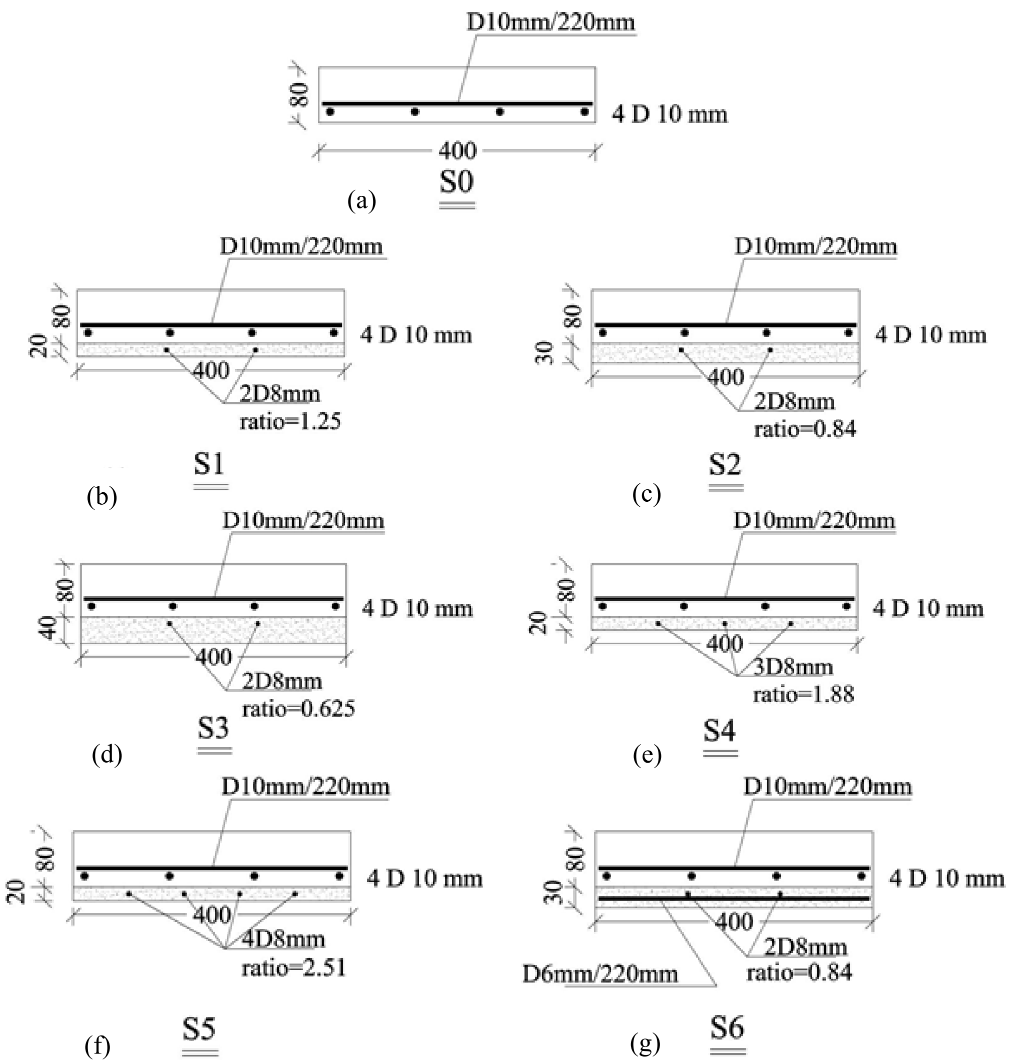

Fig. 3 Geometry and reinforcement of the RC slabs

2.3 Strengthening schemes

Geometry and reinforcement details for all RC slabs were depicted in Fig. 3. The experimental methodology was considered strengthening the whole length of the tensile side of the RC slab. The variable parameters were the thickness and the reinforcement ratio of the SHCC layer. Specimens S1, S4, and S5 were strengthened with the same thickness of SHCC layer which equal 20 mm but differed in the longitudinal reinforcement ratio of the layer. On the other hand, specimens S2 and S6 were strengthened with a 30 mm SHCC layer. Specimen S3 was strengthened with a 40 mm SHCC layer. As shown in Fig. 3(g), only specimen

Table 3 Details of the tested specimens

Slab ID	Dimensions of SHCC layer		Reinforcement of SHCC layer			
	Thickness (mm)	width (mm)	Longitudinal RFT		Transversal RFT	
			No. of bars	ratio %	No. of bars	ratio %
S0	---	---	-----	-----	-----	-----
S1	20	400	2D8	1.26	-----	-----
S2	30	400	2D8	0.84	-----	-----
S3	40	400	2D8	0.63	-----	-----
S4	20	400	3D8	1.88	-----	-----
S5	20	400	4D8	2.51	-----	-----
S6	30	400	2D8	0.84	8D6	0.42

(a) the wood form used in the casting.

(b) paint the oil before of reinforcing steel.

(c) the reinforcement shape into the form.

(d) using of the vibrator.

(e) shape of the slabs after casting.

Fig. 4 Manufacturing process of cast-in-situ the RC slab specimens

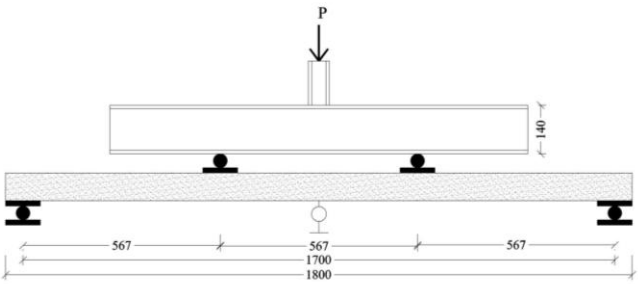

Fig. 5 Test setup and instrument (All dimensions in mm)

S6 had SHCC layer which contained longitudinal and transversal reinforcement. Table 3 shows dimension and reinforcement ratio of SHCC layer for all tested slabs.

Fig. 4 shows the followed consecutive steps to produce the RC slabs. For the strengthening procedure, firstly, the tension soffit of the RC slab was well grinded and a wooden form was fixed around it to ensure the required SHCC layer thickness. Secondly, the RC slab surface was well cleaned and the strengthening SHCC layer was cast with the required thickness. Finally, the reinforcing bars were added within the SHCC layer and its surface was well evened. Curing of the strengthened RC slabs continued up to 15 days using wet towels of the wool to prevent the shrinkage cracks.

2.4 Test setup

The experimental set-up was shown in Fig. 5. The full-scale RC slabs were tested under a four-point loading scheme. The two hinged supports were carried out using rigid steel plates which had dimension of 400x100x30 mm. The vertical deflection at middle span of the RC slab was recorded using a 50 mm displacement gauge with an accuracy of 0.01 mm. The RC slabs were tested under the load control using a hydraulic jack with a capacity of 250 kN. A low loading rate of 0.5 kN/ 1 minute was applied in the experiment in order to easily mark the observed cracks. A rigid steel beam was used to transmit the jack load to the beam. Two loading steel plates had size of 400×100×30 mm were placed under the rigid beam to distribute the applied load uniformly over the concrete surface to avoid the stress concentration.

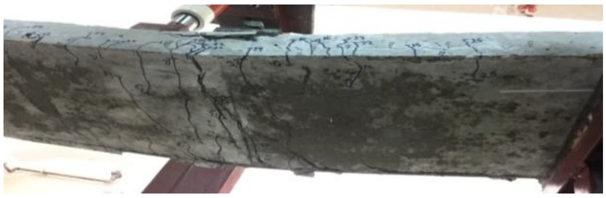

Fig. 6 Cracks pattern of the bottom side for specimen S0

Fig. 7 Failure pattern for specimen S0

3. Experimental results and discussions

3.1 Cracks propagation and failure modes

The experimental investigation showed that the first crack (P_{cr}) of the control specimen (S0) appeared at the middle part of the bottom side at 8 kN. The deflection at the cracking load (Δ_{cr}) was about 5.01 mm while the stiffness (k) was equal to 1.02 kN/mm. As the applied load increased, the number of the cracks increased and spread

Fig. 8 Failure pattern for specimen S1

Fig. 9 Failure pattern for specimen S4

Fig. 10 Failure pattern for specimen S5

along the slab length, as shown in Fig. 6. At applied load equal to 22 kN, the concrete cover spilt along the bottom steel reinforcement. The concrete cover splitting continued till the ultimate failure load (P_u) of the specimen. The RC control slab S0 failed under flexural cracks followed by the compression failure occurred under the right loading plate, as depicted in Fig. 7.

On the other side, the cracking loads of the RC slab specimens S1, S4, and S5 were 11, 13, and 10 kN, respectively. It is noted that the first crack of these specimens appeared at the same load level approximately. On the contrary, there was a significant difference in the cracking load of the SHCC layer due to the dissimilarity of the additional reinforcement ratio. The cracking loads of the SHCC layer of specimens S1, S4, and S5 were 2, 10, and 5 kN, respectively. Stiffness of the specimen S5 was the highest compared to all strengthened specimens and equal to 3.4 kN/mm because it contained the highest reinforcement ratio embedded in the strengthening layer. Δ_{cr} of specimen S4 was 9.50 mm and equal 9.10 mm, and 6.30 mm for specimens S1 and S5, respectively. Specimens S1, S4, and S5 failed under compression failure, as shown in Fig. 8, Fig. 9 and Fig. 10.

The first crack of the RC slab and SHCC strengthening layer of specimen S2 appeared at the same load level equal to 3 kN. RC slab of specimen S6 had the highest cracking load which equal 26.3 kN with 228% increasing ratio compared to the control specimen. This referred to the reinforcement mesh in orthogonal directions which helped in delaying the formation of the first crack on the slab soffit. The SHCC layer of specimen S6 cracked earlier than the RC slab at the cracking load of 4.6 kN. As the applied load increased, horizontal cracks appeared caused the splitting of the concrete cover. Δ_{cr} of the specimens S2 and S6 was 3.10 and 15.85 mm while their stiffness was 1.28 and 2.84 kN/mm, respectively. Specimen S2 failed due to debonding

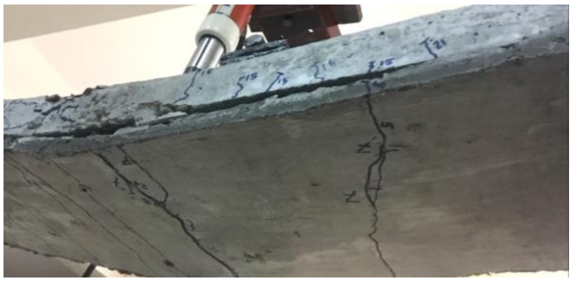

Fig. 11 Failure pattern for specimen S2

Fig. 12 Failure pattern for specimen S6

Fig. 13 Failure pattern for specimen S3

of SHCC layer, as shown in Fig. 11. The debonding started at the mid-span and propagated toward to the supports. Specimen S6 failed by the concrete cover splitting followed by the compression failure in the RC slab due to high resistance of the tension side, as depicted in Fig. 12.

In case of specimen S3, the first crack of the RC slab appeared at 13 kN at the bottom soffit while it appeared at 5 kN in case of the strengthening layer. Deflection at the cracking load was 9.40 mm while it was 5.01 mm in case of the control specimen. This may be due to the high thickness of the strengthening layer. Stiffness of S3 was 1.39 kN/mm. Specimen S3 failed by debonding of the SHCC layer in the mid span zone followed by the compression failure under the loading plate, as shown in Fig. 13.

3.2 Load-deflection responses

The tested specimens were divided into three groups to be compared together. The first one contained three specimens (S1, S4, and S5) had the same thickness of the strengthening layer which equal 20 mm in addition to the control specimen S0. The second group involved S2 and S6 with 30 mm SHCC layer besides the control specimen. Finally, specimens S1, S2, and S3 had the same SHCC reinforcement value (2D8), plus the control specimen had been listed in the third group. Table 4 concluded the results of the tested specimens.

For the first group, as the reinforcement ratio within the SHCC layer increased, both the ultimate failure load (P_u) and the deflection at the failure (Δ_u) increased, as shown in Fig. 14. The additional reinforcement bars can uniformly

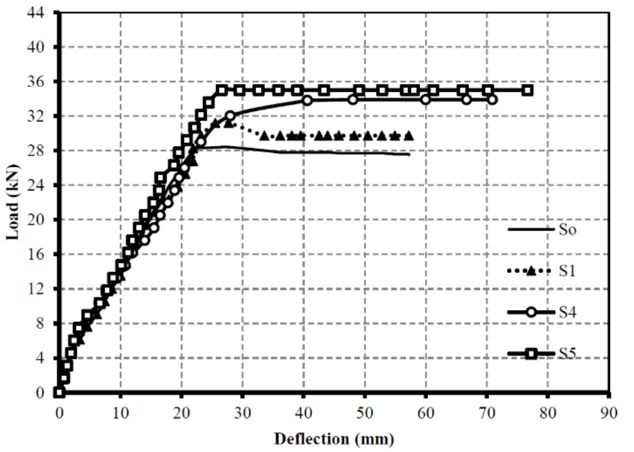

Fig. 14 Load deflection behavior of specimens S0, S1, S4, and S5

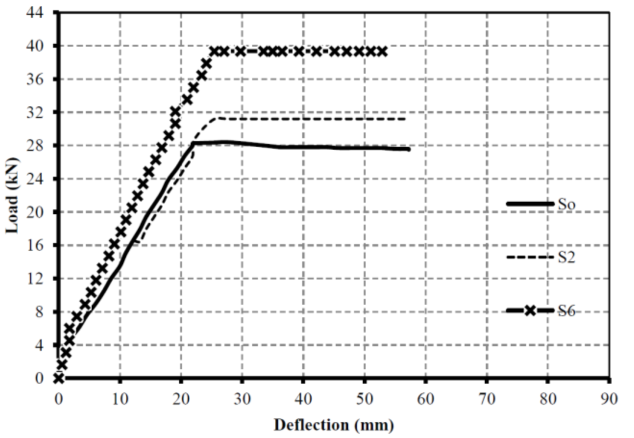

Fig. 15 Load deflection behavior of specimens S0, S2, and S6

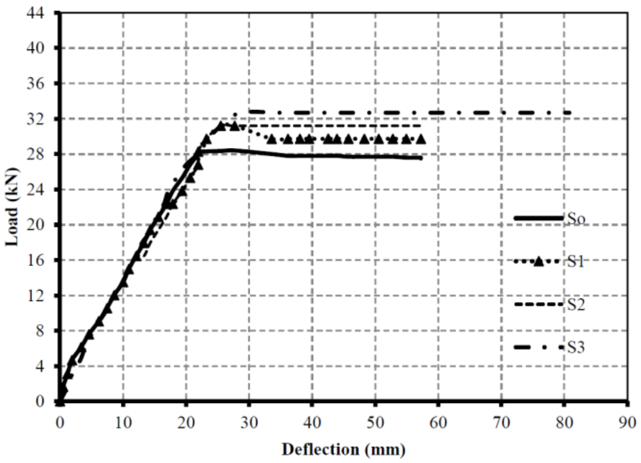

Fig. 16 Load deflection behavior of specimens S0, S1, S2 and S3

distribute the stress along the slab span and delay the crack formation which helped in increasing the capacity of the strengthened RC slab. The ultimate failure load of the specimens S1, S4, and S5 increased by 11, 18, and 25% compared to the control specimens while their deflections at the failure were 55, 72, and 77 mm, respectively. The

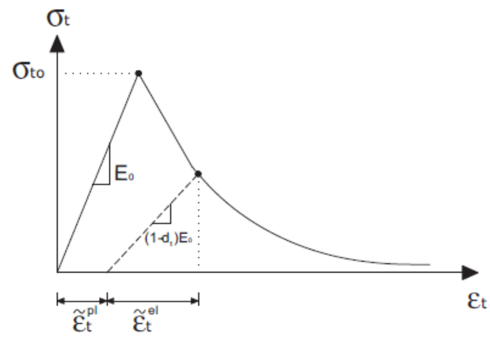

(a)

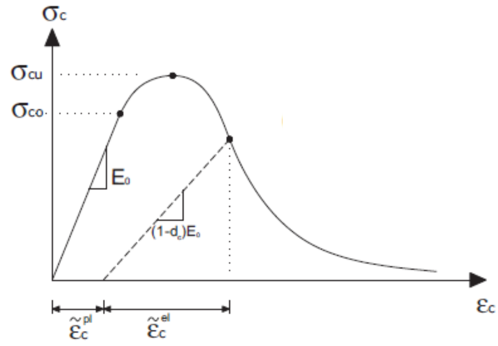

(b)

Fig. 17 Stress-strain curve of the concrete (a) tension and (b) compression, Hibbitt *et al*. (2000)

strengthening pattern in this group reflected the efficiency of the 20 mm reinforced SHCC layer in improving the capacity and the failure deflection of the RC slabs.

The load deflection responses of the second group specimens were shown in Fig. 15. Specimen S2 and S6 had the same SHCC thickness and longitudinal reinforcement ratio. The strengthening layer of specimen S6 contained the transversal reinforcement which is not available in case of the specimen S2. The ultimate load of the two specimens was quite different. Specimen S6 failed at 35 kN which was 25% higher than the control specimen, while the specimen S2 failed at 31 kN with increasing ratio of 11% compared to the control slab. The ultimate load of the specimen S2 was lower than that of S6 because it failed under debonding of the strengthening layer hence the full capacity was not reached. Deflections at the failure were 60 and 55 mm for S2 and S6, respectively.

The load-deflection curves of the third group were drawn in Fig. 16. Despite that the S3 specimen had the highest thickness of the strengthening layer, it had not the highest ultimate load capacity compared to the group specimens. This may because the S3 failed due to the debonding of the strengthening layer. Specimen S3 failed at 33 kN which was 18% higher than that of the control specimen. On the contrary, the failure deflection of specimen S3 was the highest among the tested specimens. It failed at 83 mm compared to 57 mm in case of the control slab due to the high thickness of the strengthening layer.

3.3 Ductility analysis

The efficiency of the proposed strengthening material

Table 4 Test results of the tested specimens

Beam	P_{cr} (kN)		Δ_{cr} (mm)	Stiffness (kN/mm) (k=P/Δ)	P_u (kN)	Increase in P_u%	Δ_y (mm)	Δ_u (mm)	Ductility Index (Δ=Δ_u/Δ_y)	Increase in the ductility index %
	RC slab	UHP -SHCC								
S0	8	---	5.01	1.02	28	---	22	57	2.59	---
S1	11	2	9.10	1.15	31	11	18	55	3.06	18.2
S2	3	3	3.10	1.28	31	11	19	60	3.16	22.0
S3	13	5	9.40	1.39	33	18	29	83	2.87	10.8
S4	13	10	9.50	1.41	34	18	25	72	2.88	11.2
S5	10	5	6.30	3.40	35	25	26	77	2.97	14.7
S6	26.3	4.6	15.85	2.84	35	25	20	55	2.75	6.2

should be evaluated on the level of improving the ultimate load along with enhancing the ductility of the RC slabs. The previous section 3.2 discussed the ability of the reinforced layer of the SHCC to increase the ultimate load of the strengthened slabs. Herein, a ductility analysis was investigated to show the effect of the SHCC on the ductility of the strengthened slabs. The ductility index (Δ) was defined as the ratio between the deflection at the ultimate load (Δ_u) to the deflection at the yield load (Δ_y) for each slab. Table 4 listed the ductility index and the increasing ratio of the ductility index for the strengthened specimens compared to the control specimen.

It was shown that the ductility indexes of all strengthened RC slabs were greater than the ductility index of the control slab. It reflected the efficiency of the PE fiber used in the SHCC layer in distributing the cracks along the whole span of the RC slab and prevented propagation of the crack width. In addition, the use of reinforcing bars in the SHCC layer significantly contributed in increasing the ductility of the strengthened slabs with respect to the control slab. The ductility indexes of the strengthened specimens ranged from 2.75 to 3.16 compared to 2.59 in case of the control slab. Specimen S2 had the largest increasing ratio of the ductility index compared to the control slab which equal 22%, while the increasing ratio of the other specimens ranged from 6.2 to 18.2%.

4. Numerical analysis

The flexural behavior of RC slabs strengthened with SHCC was analyzed numerically by a three-dimensional (3D) non-linear finite element model carried out using the finite element modeling software ABAQUS/standard. Results of the numerically analyzed RC slabs strengthened with SHCC layers were compared against the experimental responses to validate the proposed finite element model. Furthermore, many variables that affect the flexural behavior of RC slabs strengthened with SHCC layers were analyzed.

4.1 Material properties

4.1.1 Concrete and UHP-SHCC

The concrete damage plasticity model was used to simulate the behavior of the concrete and the UHP-SHCC. The used model assumes that the main two failure modes are the tensile cracking and the compressive crushing (Hibbitt *et al*. 2000). In case of uniaxial tension, the stress-strain relationship obeys a linear elastic correlation till the value of the failure stress is achieved; the failure stress corresponds to the onset of micro cracking in the concrete material. After the failure stress, the formation of micro-cracks is represented with a softening stress-strain relationship. Under uniaxial compression, the response is typically represented by strain hardening followed by strain softening beyond the ultimate stress.

Fig. 17 shows the uniaxial tensile and compressive curves of the concrete according to the damaged plasticity. The degradation of the elastic stiffness is classified by two damage variables, d_t and d_c, which are assumed to be functions of the plastic strains, temperature, and field variables as illustrated below in the Eqs. (1) and (2), respectively

$$d_t = d_t\left(\varepsilon_t^{\simeq pl}, \theta, f_i\right): 0 \leq d_t \leq 1 \tag{1}$$

$$d_c = d_c\left(\varepsilon_c^{\simeq pl}, \theta, f_i\right): 0 \leq d_c \leq 1 \tag{2}$$

The damage variables can take values from zero, representing the undamaged material, to one, which represents the total loss of the strength. If E_0 is the initial (undamaged) elastic stiffness of the material, the stress-strain relations under uniaxial tension and compression loading are estimated using Eqs. (3) and (4), respectively

$$\sigma_t = (1 - d_t)E_0\left(\varepsilon_t - \varepsilon_t^{\simeq pl}\right) \tag{3}$$

$$\sigma_c = (1 - d_c)E_0\left(\varepsilon_c - \varepsilon_c^{\simeq pl}\right) \tag{4}$$

According to Egyptian code ECP 203-2017, the following Eq. (5) was used to calculate the elasticity modulus (E_0) of the concrete and the SHCC.

$$E_0 = 4400\sqrt{\sigma_{cu}} \tag{5}$$

Where σ_{cu} is the compressive strength of the concrete and the SHCC, as listed in Table 2. Values of the E_0 of the concrete and the SHCC were listed in Table 5.

Poisson's ratio for both concrete and SHCC were assumed and shown in Table 5. Stress-strain relationships in the compression and the tension for the concrete and the SHCC that incorporated in the proposed finite element model were obtained by Saenz model 1964, as drawn in Fig. 18. In the current modeling, the linear behavior of the concrete was assumed in the elastic stage. The required items in this stage were the elasticity modulus and

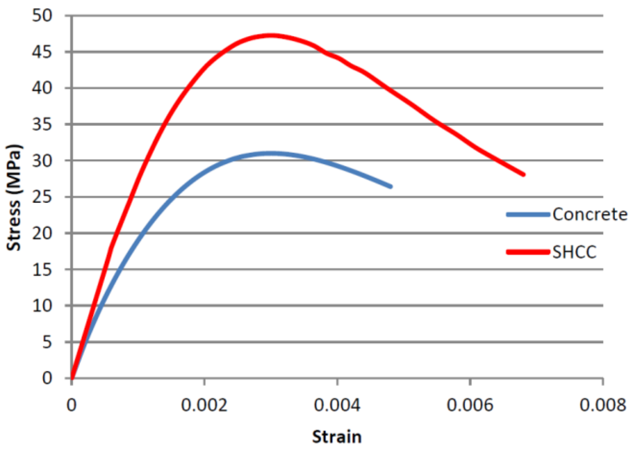

(a)

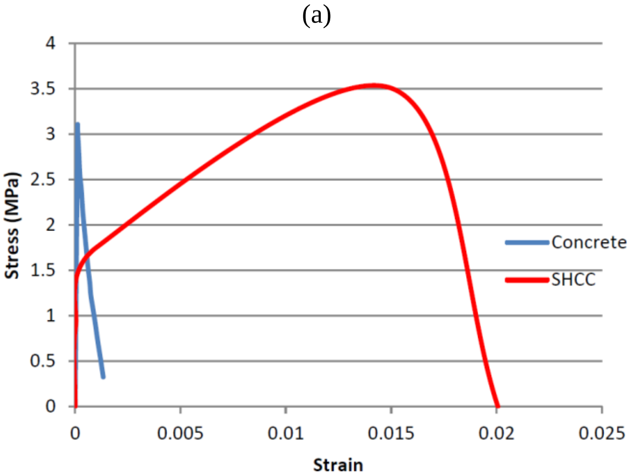

(b)

Fig. 18 Stress–strain modeling of the concrete and the SHCC incorporated in the proposed finite element model : (a) In compression and (b) In tension

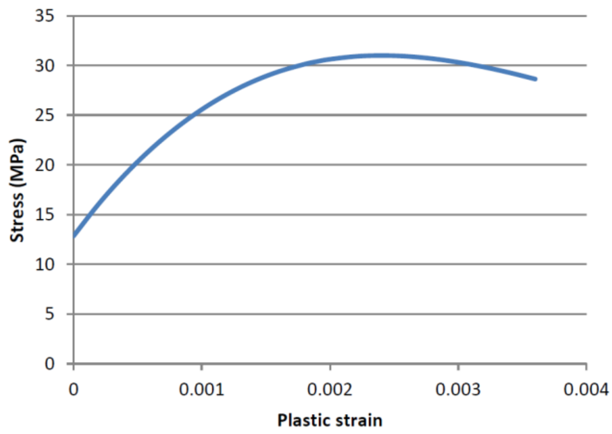

(a)

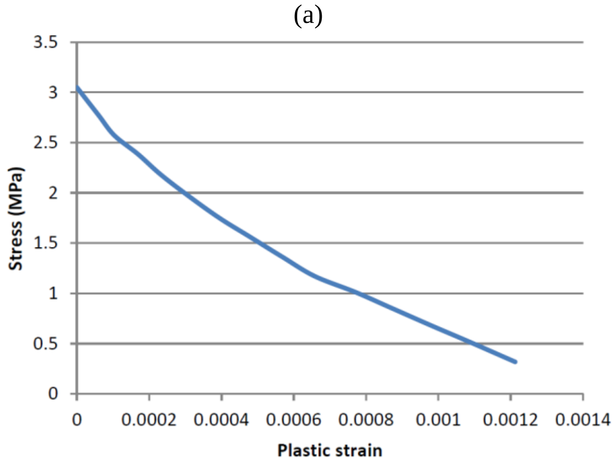

(b)

Fig. 19 Non-linear behavior of concrete: (a) In compression and (b) In tension

Poisson's ratio. On the other hand, the non-linear behavior of the concrete in the tension as well as in the compression, as shown in Fig. 19, were used in the plastic stage. For SHCC modeling, the required items in the elastic stage were the elasticity modulus and Poisson's ratio and these values were listed in Table 5. The compressive stress-strain response of the SHCC in the plastic stage was simulated within the finite element modeling as depicted in Fig. 20. The plastic strains of the horizontal axis of Fig. 19(a) and Fig. 20 were estimated as equal the strains of Fig. 18 minus 15% of the ultimate strain. The tensile stress-strain response of the SHCC was based on the zero-span tensile model that proposed by Zhang *et al*. (2013) and in conformity with (Esmaeeli 2015). Fig. 21 illustrated the tensile stress-strain response of the SHCC. The tensile strength of SHCC was 3.50 MPa while the tensile strain at ultimate stress was 0.015. The concrete damage plasticity model parameters for the concrete and the SHCC materials were defined within the proposed finite element model, as listed in Table 6.

4.1.2 Steel reinforcement

The steel rebars were modeled using the current experimental measurements. The elastic modulus of the steel reinforcement was 200 GPa. Moreover, the yield stress of the HTS and the NMS were 410 MPa and 245 MPa, respectively. A Poisson's ratio of 0.3 was selected for the steel reinforcement. The bond between the steel reinforcement and the concrete was simulated as a perfect bond (embedded region). In the embedded region modeling, the bond slip between the rebar surface and the surrounded concrete is not considered and this concept goes with the current study. The truss element is the most famous method to model the reinforcement and it only requires a cross-sectional area of the rebar. The steel reinforcement was modeled as a truss element.

4.1.3 UHP-SHCC/ concrete interface

A cohesive surface model was used to represent the interface between the concrete and the SHCC to capture the debonding failure mode which occurred in the experiments. It was impossible to be simulated by using the perfect bond model. The cohesive behavior was simulated in terms of the traction versus the separation. It allowed consideration of the cohesive parameters as a function of the normal to shear displacements ratio at the bonding interface. Also, it assumed a linear elastic traction-separation law prior to the damage. Three zones were necessary to construct the traction separation of the cohesive surface model. The first was the initial stiffness (K_o). The second was the damage initiation point (δ_0, τ_{max}). The last was the damage evolution

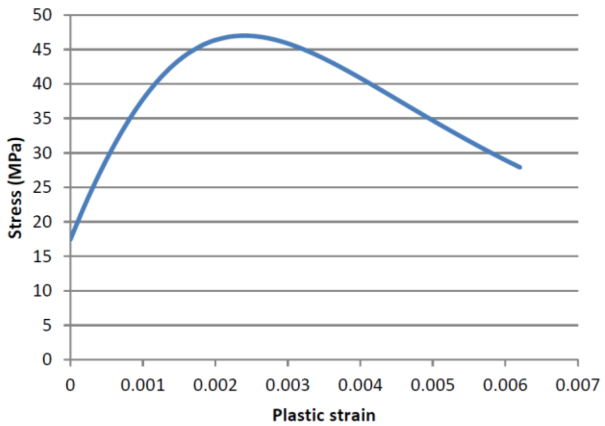

Fig. 20 Non-linear response of SHCC in compression

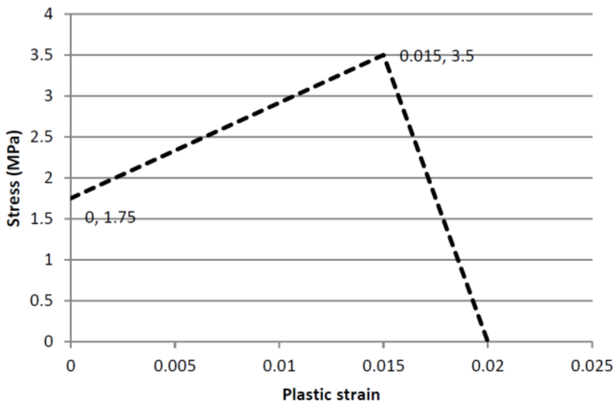

Fig. 21 Tensile response of SHCC

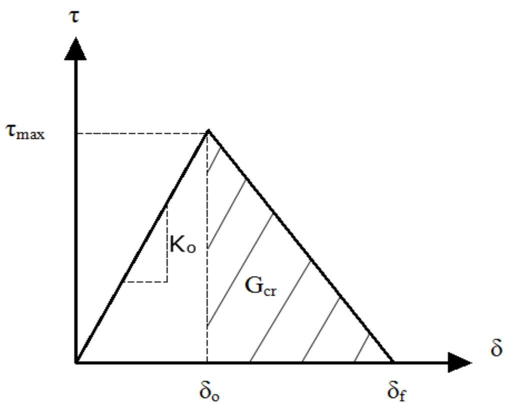

Fig. 22 Traction separation response of the cohesive surface

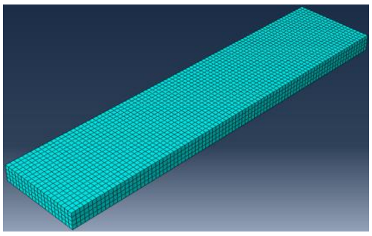

(a) Concrete elements

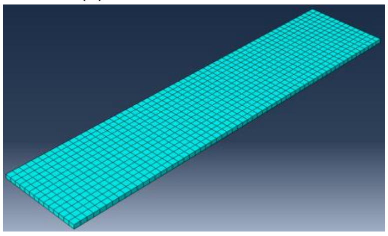

(b) SHCC elements

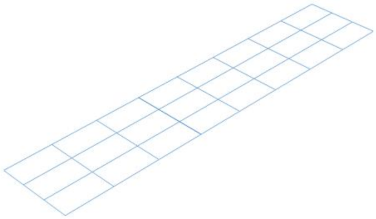

(c) Steel reinforcement elements

Fig. 23 The used mesh size

Table 5 Parameters of the concrete and the SHCC

Property	Source	Concrete	SHCC
Compressive strength (MPa)	Current experiments	31	47
Tensile strength (MPa)	Current experiments	3.05	3.5
Modulus of elasticity (GPa)	Calculated according ECP 203-2017	25.5	30
Poisson's ratio	Assumed	0.2	0.22

zone (G_{cr}), as depicted in Fig. 22. Traction separation response of the cohesive surface was drawn in Fig. 22 where the horizontal axis represented the normal strength and the vertical axis represented the shear strength. It is clear that the relationship between the traction stress and the effective opening displacement was represented by the initial stiffness (K_o), the material strength (τ_{max}), the displacement at the fracture (δ_f) and the fracture energy (G_{cr}). The G_{cr} was equal to the area under the traction-separation curve after the peak point. The initial stiffness K_o was defined using Eq. (6).

$$K_o = \frac{G_c}{t_c} \tag{6}$$

Where t_c was the concrete cover (25 mm) and G_c was the shear modulus of the concrete. The G_c was calculated from the following Eq. (7).

$$G_c = \frac{E_0}{2(1+\mu)} \tag{7}$$

Where E_0 was the elasticity modulus of the SHCC layer (30 GPa) and μ was poison ratio (0.22).

The G_c equaled 12.29 GPa. Also, in this study, τ_{max} was considered to be 0.6 MPa and G_{cr} =900 J/m^2, as recommended by Obaidat *et al*. (2010).

4.2 Elements, boundary conditions and mesh size of FEM

An eight-noded linear brick element (C3D8R) was used to model the concrete, the SHCC and the loading plates. A two-noded linear 2D truss element (T3D2) was used in modeling the steel reinforcement, as depicted in Fig. 23. The used mesh size was chosen based on the numerical trials with mesh sizes ranged from 1.0 to 5.0 cm^2. In the current study, a fine mesh with maximum area of 3.0 cm^2 was used because a finer mesh did not show a significant

Table 6 Concrete damage plasticity model parameters of the concrete and the SHCC

Material	Dilation angle	Eccentricity	$\frac{f_{b0}}{f_{c0}}$	K	Viscosity parameter
Concrete	20	0.1	1.16	0.667	0
SHCC	36	0.1	1.16	0.667	0

Table 7 Model size and CPU time

Beam ID	Number of elements	Degree of freedom (DOF)	CPU time (minutes)
S0	3080	13758	45
S1	4951	22347	65

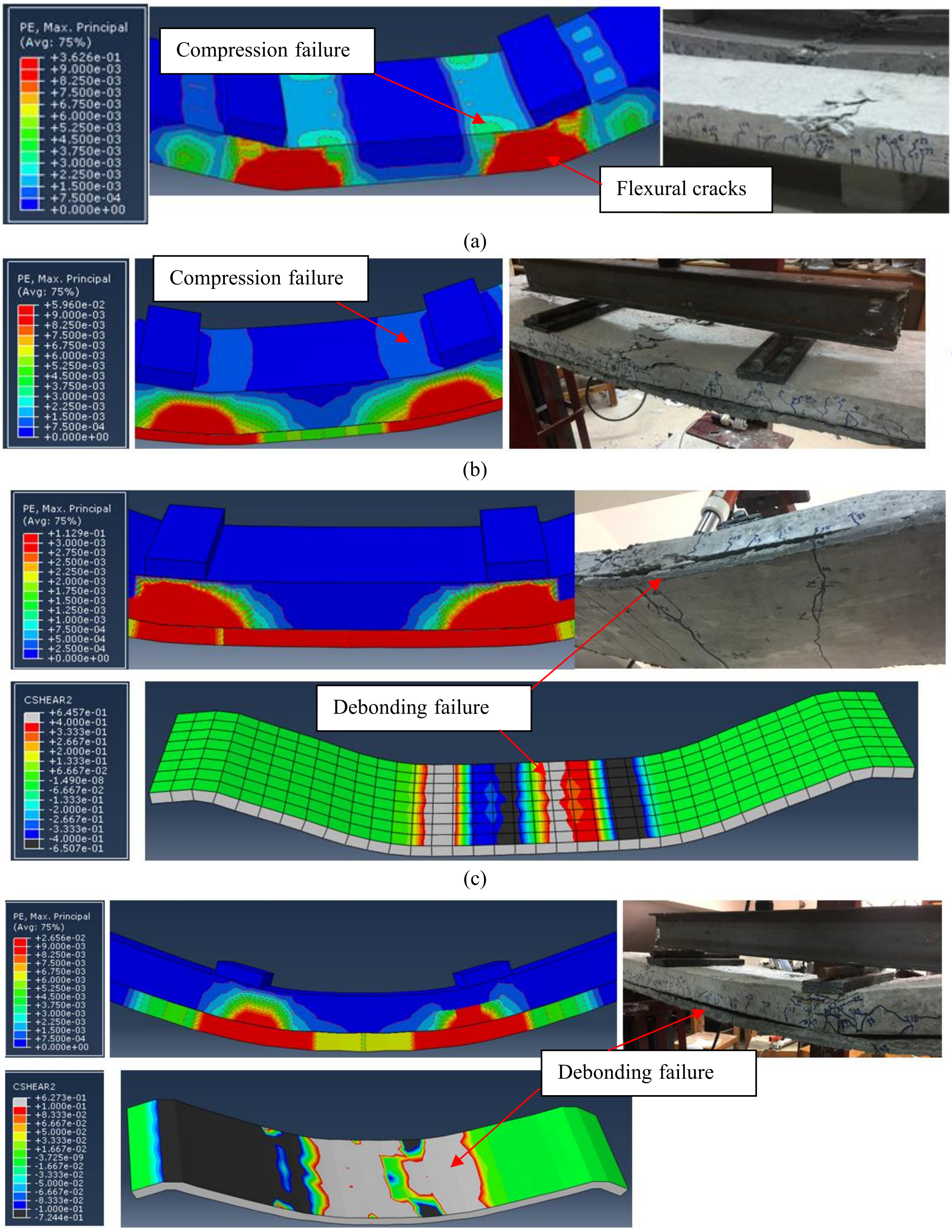

Fig. 25 Numerical versus experimental failure pattern: (a) So, (b) S1, (c) S2, (d) S3 (e) S4 (f) S5, and (g) S6

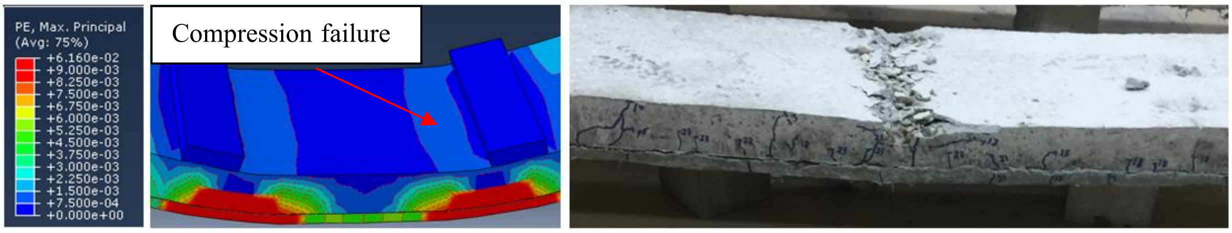

(e)

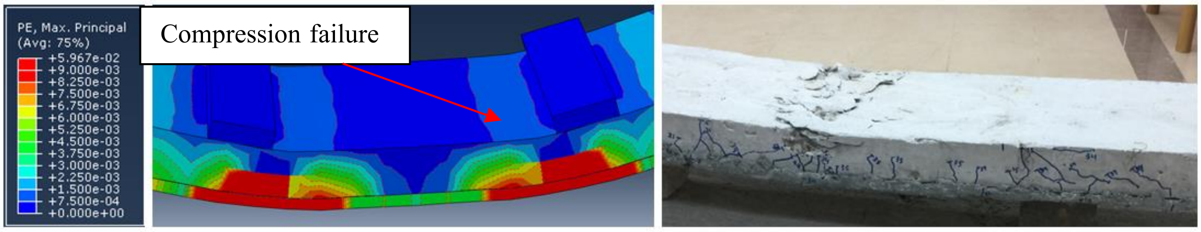

(f)

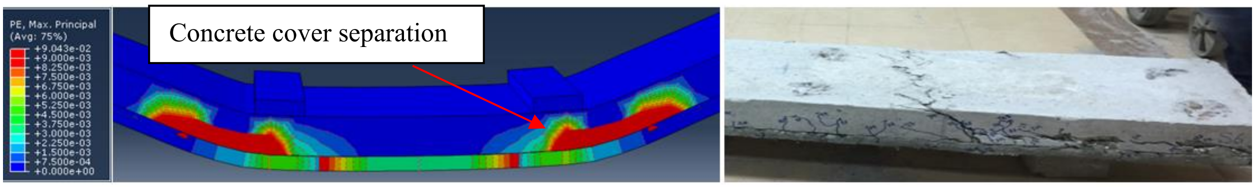

(g)

Fig. 25 Continued

difference in the results. In order to display the shear stress on the specimen's width, which caused the debonding on the concrete/SHCC interface, a 3D finite element model with hinged-hinged supports was proposed. Table 7 showed number of the elements and number of the degrees of freedom for some specimens. The loading was applied using a quasi-static analyzing technique with a monotonic increasing force. The force was applied at the top of the RC slab. Specimens had been analyzed using four-point bending system. The steel loading plates had been tied up with the specimens' surfaces to remove the stress concentrations around the points of the loading and the supports.

5. Numerical validation

In this section, the numerical results obtained using the finite element model were compared to the experimental responses to check its accuracy. Fig. 24 showed that the numerical and the experimental load-deflection behavior of all slabs. Two results were in a good manner. Also, Table 8 listed values of the ultimate loads and the ultimate deflections of all slabs. It was concluded that the numerical finite element well predicted the behavior of the analyzed specimens on the levels of the ultimate load and the deflection at failure. The ratio between the experimental ($P_{u,\ \mathrm{exp}}$) and the numerical ($P_{u,\ \mathrm{num}}$) ultimate loads ranged from 0.87 to 1.00. The ratio between the experimental ($\Delta_{u,\ \mathrm{exp}}$) and numerical ($\Delta_{u,\ \mathrm{num}}$) deflection at the failure ranged from 0.93 to 1.04. In addition, there was a match across the load-deflection curve of each specimen. The numerical model not only able to predict the load deflection behavior of the analyzed RC slabs, but also it can effectively capture the failure mode, as shown in Fig. 25. Fig. 25(a) showed the flexural cracks followed by the compression failure of the control slab. The compression failure patterns occurred in the specimens S1, S4, and S5, as obviously depicted in Fig. 25(b), Fig. 25(e), and Fig. 25(f), respectively. On the other hand, Fig 25(c) and Fig 25(d) showed the numerical intermediate debonding failure pattern at the mid-span zone for the specimens S2 and S3 which well agreed with the experimental failure patterns. Finally, Fig. 25(g) showed the numerical and experimental concrete cover separation which occurred in case of the specimen S6.

6. Parametric study

The validated FEM was used to run a parametric analysis. Three parameters were numerically studied. The first was effect of the additional reinforcement ratio of the SHCC layer. The second was the layer thickness. The last was using the steel connectors to adjoin the concrete/SHCC interface. The numerical investigation included effect of these parameters on the behavior of the strengthened slabs.

6.1 Effect of the reinforcement ratio within the SHCC layer

This section investigated the effect of the reinforcement ratio within the SHCC layer on the behavior of the slabs. A new 12 RC slab specimens with different ratios of the additional reinforcement ratio of the SHCC layer were

Table 8 Comparison between the numerical and experimental results

Beam	P_u (kN) Experimental $P_{u,\text{exp}}$ (kN)	Numerical $P_{u,\text{num}}$ (kN)	$P_{u,\text{exp}}$/ $P_{u,\text{num}}$	Δ_u (mm) Experimental Δu, exp (mm)	Numerical Δu, num (mm)	Δu, exp/ Δu, num
S0	28	29	0.96	57	60	0.95
S1	31	31.2	0.99	55	59	0.93
S2	31	31.9	0.97	60	60	1.00
S3	33	34	0.97	83	80	1.04
S4	34	34	1.00	72	74	0.97
S5	35	36.5	0.95	77	80	0.96
S6	35	40	0.87	55	55	1.00

Table 9 Reinforcement ratio for the analyzed specimens

Slab ID	Dimensions of SHCC layer		Reinforcement of SHCC layer			
			Longitudinal RFT		Transversal RFT	
	Thickness (mm)	width (mm)	No. of bars	ratio %	No. of bars	ratio %
S0	---	---	-----	-----	-----	-----
S1	20	400	2D8	1.26	-----	-----
R1	20	400	4D8	2.52	-----	-----
R2	20	400	4D10	3.93	-----	-----
S2	30	400	2D8	0.84	-----	-----
R3	30	400	4D8	1.68	-----	-----
R4	30	400	4D10	2.62	-----	-----
S3	40	400	2D8	0.63	-----	-----
R5	40	400	4D8	1.26	-----	-----
R6	40	400	4D10	1.96	-----	-----
S4	20	400	3D8	1.88	-----	-----
R7	20	400	6D8	3.77	-----	-----
R8	20	400	6D10	5.89	-----	-----
S5	20	400	4D8	2.51	-----	-----
R9	20	400	8D8	5.02	-----	-----
R10	20	400	8D10	7.85	-----	-----
S6	30	400	2D8	0.84	8D6	0.42
R11	30	400	4D8	1.67	8D6	0.42
R12	30	400	4D10	2.62	8D6	0.42

modeled. Table 9 showed the analyzed 12 RC slab specimens using the validated numerical model in addition to the 7 tested specimens. The specimen S3 had the least ratio of 0.63 % while the specimen R10 had the highest ratio of 7.85 %. The numerical results of the analyzed slabs can be found in Table 10. It was can be noted that, the increase of the SHCC reinforcement ratio did not improve significantly the ultimate load capacity of the specimens that failed under the compression failure: S1, S4, and S5, as depicted in Fig. 26. On the other hand, the two specimens S2 and S3 failed due to the debonding of the SHCC layer. S2 and S3 showed a different behavior with increasing the SHCC reinforcement ratio. In case of specimen S3, the SHCC layer was completely debonded at the failure load which explained why the ultimate failure load of the specimens R5 and R6 were approximately equal to the ultimate failure load of specimen S3. On the contrary, the SHCC layer of specimen S2 debonded only in the middle span zone which reflected the possibility of increasing the ultimate load with the increase of the SHCC reinforcement ratio. The ultimate load of the specimens R3 and R4 were

Table 10 Results of the analyzed RC slabs strengthened with reinforced SHCC layers using different reinforcement ratios

Beam	P_u (kN)	Increase in P_u%	Δ_y (mm)	Δ_u (mm)	Ductility Index (Δ=Δ_u/Δ_y)	Increase in the ductility index %	Failure mode
S0	29	---	22	60	2.73	---	Flexural cracks followed by compression failure
S1	31.2	7.6	18	59	3.28	20.19	Compression Failure
R1	31.7	9.3	20	60	3.00	10.00	Compression Failure
R2	32.3	11.4	21	62	2.95	8.25	Compression Failure
S2	31.9	10	19	60	3.16	15.79	Debonding of the SHCC layer
R3	34.6	19.3	20	66	3.3	20.88	Debonding of the SHCC layer
R4	36	24.2	21	72	3.42	25.27	Debonding of the SHCC layer
S3	34	17.2	29	80	2.76	1.15	Debonding of the SHCC layer
R5	34.1	17.6	29	81	2.79	2.41	Debonding of the SHCC layer
R6	34.2	17.9	30	82	2.73	0.22	Debonding of the SHCC layer
S4	34	17.2	25	74	2.96	8.53	Compression Failure
R7	34.3	18.3	25	75	3.00	10.00	Compression Failure
R8	34.7	19.7	26	76	2.92	7.18	Compression Failure
S5	36.5	25.9	26	80	3.08	12.82	Compression Failure
R9	36.6	26.2	29	81	2.79	2.41	Compression Failure
R10	36.8	26.9	29	81	2.79	2.41	Compression Failure
S6	40	37.9	20	55	2.75	0.83	Concrete cover splitting
R11	48.6	67.6	22	70	3.18	16.67	Debonding of the SHCC layer
R12	50	72.4	22	71	3.23	18.32	Debonding of the SHCC layer

34.6 and 36 kN while it was 31.9 kN for the specimen S2. The high reinforcement ratio within the SHCC not only improved the ultimate load but also enhanced the ductility of specimens R3 and R4. The increasing ratio of the ductility index of the specimens S2, R3, and R4 were 15.79, 20.88, and 25.27%, respectively, compared to the control specimen S0. This reflected the efficiency of the proposed strengthening techniques. Moreover, the failure pattern of the specimen S6 changed from the concrete cover splitting to the debonding of the SHCC layer. The reason was the increase of the SHCC reinforcement ratio which caused a significant increase in both the ultimate load and the ductility index. The increasing ratio of the ultimate load of

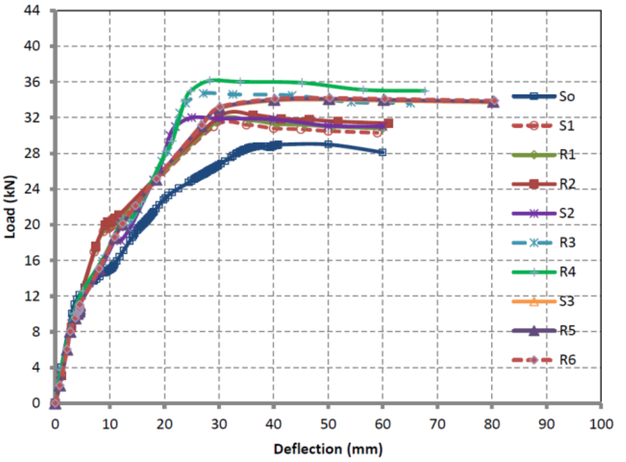

(a)

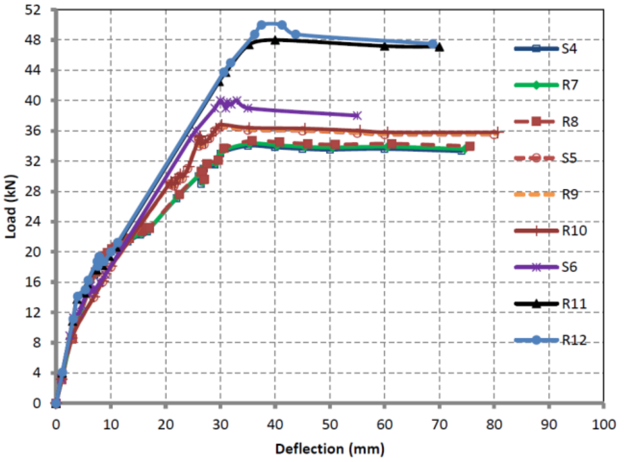

(b)

Fig. 26 The numerical load deflection responses: (a) specimens So, S1, R1, R2, S2, R3, R4, S3, R5 and R6, (b) specimens S4, R7, R8, S5, R9, R10, S6, R11 and R12

the specimens S6, R11, and R12 were 37.9, 67.6, and 72.4% referenced to the S0 while the increasing ratio of the ductility index of these slabs were 0.83, 16.67, and 18.32%, respectively.

6.2 Effect of the thickness of the SHCC layer

To explain the effect of the SHCC layer thickness on the behavior of the strengthened RC slabs, 17 specimens were analyzed using the FEM. The geometry of these slabs were shown in Table 11. The thickness ranged from 10 mm which equal 12.5% of the slab depth to 60 mm which equal 12.5% of the slab depth. The 17 numerical slabs were derived from the 7 experimental slabs. Table 12 listed values of the ultimate loads and deformations of all slabs.

It was noticed that the specimens with 10 mm thickness of SHCC layer did not improve the ultimate failure load significantly compared to the control specimen due to the rupture of the strengthening layer, as depicted in Fig. 27. The increase of the SHCC layer thickness did not significantly improved the ultimate load or the ductility index for the specimens failed under the compression failure mode. On the contrary, in case of the specimens

Table 11 Dimensions of the analyzed specimens using different thickness of SHCC layers

Slab ID	Dimensions of SHCC layer		Reinforcement of SHCC layer	
	Thickness (mm)	Width (mm)	Longitudinal RFT ratio %	Transversal RFT ratio %
S0	---	---	-----	-----
T1	10	400	1.26	-----
S1	20	400	1.26	-----
T2	40	400	1.26	-----
T3	60	400	1.26	-----
T4	10	400	0.84	-----
S2	30	400	0.84	-----
T5	40	400	0.84	-----
T6	60	400	0.84	-----
T7	10	400	0.63	-----
S3	40	400	0.63	-----
T8	60	400	0.63	-----
T9	10	400	1.88	-----
S4	20	400	1.88	-----
T10	40	400	1.88	-----
T11	60	400	1.88	-----
T12	10	400	2.51	-----
S5	20	400	2.51	-----
T13	40	400	2.51	-----
T14	60	400	2.51	-----
T15	10	400	0.84	0.42
S6	30	400	0.84	0.42
T16	40	400	0.84	0.42
T17	60	400	0.84	0.42

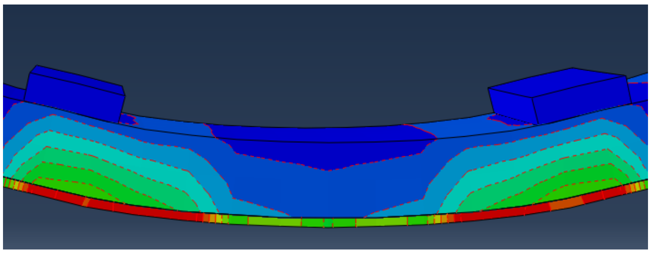

Fig. 27 The numerical failure pattern of specimen T1

failed due to the debonding of the SHCC layer, the increase of the SHCC thickness contributed in delaying of the debonding load. The ultimate load and the ductility index of the specimens T5 and T6 remarkably enhanced compared to the specimen S2. The increasing ratio of the ultimate load of the specimens S2, T5, and T6 were 10, 46.2, and 49.7% compared to the S0. The increasing ratio of the ductility index of these specimens were 15.75, 17.58, and 38.10%, respectively.

As the SHCC layer thickness increased from 30 to 40 mm, the failure pattern converted from the concrete cover splitting in the specimen S6 to SHCC debonding in the specimen T16. As a result, the ultimate load of the T16 reached 55 kN and it reached 40 kN in case of the S6. Also, the ductility index obviously improved with increasing the SHCC layer thickness. The increasing ratio of the ductility index of the specimens S6 and T15 were 0.73 and 6.96% compared to S0.

6.3 Effect of the use of the steel connectors to adjoin the concrete/ SHCC interface

Table 12 Results of the analyzed strengthened RC slabs using different thickness of SHCC layers

Beam	P_u (kN)	Increase in P_u%	Δ_y (mm)	Δ_u (mm)	Ductility Index ($\Delta=\Delta_u/\Delta_y$)	Increase in the ductility index %	Failure mode
S0	29	---	22	60	2.73	---	Flexural cracks followed by compression failure
T1	29.8	2.8	17	55	3.23	18.32	SHCC Rupture
S1	31.2	7.6	18	59	3.28	20.15	Compression Failure
T2	31.4	8.3	18	60	3.33	21.98	Compression Failure
T3	31.5	8.6	19	62	3.26	19.41	Compression Failure
T4	29.5	1.7	16	55	3.44	26.01	SHCC Rupture
S2	31.9	10	19	60	3.16	15.75	Debonding of the SHCC layer
T5	42.4	46.2	25	80	3.21	17.58	Debonding of the SHCC layer
T6	43.4	49.7	22	83	3.77	38.10	Debonding of the SHCC layer
T7	29.2	0.7	24	69	2.88	5.49	SHCC Rupture
S3	34	17.2	29	80	2.76	1.10	Debonding of the SHCC layer
T8	34.5	19	29	81	2.79	2.20	Debonding of the SHCC layer
T9	30.3	4.5	22	63	2.86	4.76	SHCC Rupture
S4	34	17.2	25	74	2.96	8.42	Compression Failure
T10	34.2	17.9	25	74	2.96	8.42	Compression Failure
T11	34.6	19.3	26	75	2.88	5.49	Compression Failure
T12	31.3	7.9	21	67	3.19	16.85	SHCC Rupture
S5	36.5	25.9	26	80	3.08	12.82	Compression Failure
T13	36.6	26.2	24	81	3.38	23.81	Compression Failure
T14	36.7	26.6	27	80	2.96	8.42	Compression Failure
T15	30	3.4	16	44	2.75	0.73	SHCC Rupture
S6	40	37.9	20	55	2.75	0.73	Concrete cover splitting
T16	55	89.7	25	73	2.92	6.96	Debonding of the SHCC layer
T17	55	89.7	24	69	2.88	5.49	Debonding of the SHCC layer

The steel connectors distributed along the longitudinal reinforcement and embedded in the RC slab with a length of 60 mm were carried out, as shown in Fig. 28. The steel connectors were used to prevent the debonding of the SHCC layer and used to enhance the mechanical behavior of the analyzed RC slabs. The steel connectors were modeled as NMS with its properties. Table 13 showed the number, the diameter, and the spacing of the used steel connectors for each analyzed RC slab. Four specimens were strengthened using a SHCC layer with connectors. The connectors fixed at the additional rebars of the layer.

The proposed strengthening techniques using the steel connectors tied both the strengthening layer and the RC slab proved its ability to prevent the debonding failure mode causing a significant increase in the ultimate load and in the

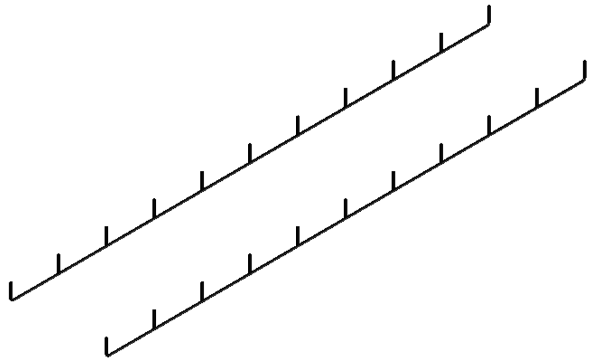

Fig. 28 The arrangement of the steel connectors of the specimen S2-SC

Table 13 Geometry of the analyzed specimens with the connectors

Slab ID	Dimensions of SHCC layer: Thickness (mm)	Dimensions of SHCC layer: width (mm)	Reinforcement of SHCC layer: Longitudinal RFT ratio %	Reinforcement of SHCC layer: Transversal RFT ratio %	Steel connectors
S0	---	---	-----	-----	-----
S2	30	400	0.84	-----	-----
S2-SC	30	400	0.84	-----	2D8@175 mm
R3-SC	30	400	1.68	-----	4D10@87.5 mm
S3	40	400	0.63	-----	-----
S3-SC	40	400	0.63	-----	2D8@175 mm
R6-SC	40	400	1.96	-----	4D10@87.5 mm

ductility index. Fig. 29. Showed the numerical failure pattern of the specimen R3-SC. The failure pattern changed from the debonding of the SHCC layer that occurred in the specimens S2 and S3 to the concrete cover splitting that occurred in the specimens R3-SC and R6-SC. This occurred because using connectors of 4D10 spaced at 87.5 mm. The increasing ratio of the ultimate load of the specimens S2, R3-SC, S3, and R6-SC were 10, 55.2, 17.2, and 44.8% compared to the S0. In addition, the increasing ratio of the ductility index of these slabs were 15.75, 15.38, 1.10, and 6.59%, respectively. On the other hand, the specimens S2-SC and S3-SC with connectors of 2D8 spaced at 175 mm had the same failure pattern (debonding of the SHCC layer) compared to the specimens S2 and S3 without steel connectors. Although, the lower amount of the steel connectors did not prevent the debonding failure mode, it delayed the debonding mechanism and increased the ultimate load of the strengthened slabs, as listed in Table 14.

7. Theoretical analysis

The nominal failure moment (M_n) of both control and SHCC strengthened RC slab specimens was obtained using a theoretical model of their cross section. The current proposed theoretical model constructed based on the

Table 14 Results of the RC slabs strengthened using SHCC layers anchored by steel connectors

Beam	P_u (kN)	Increase in P_u%	Δ_y (mm)	Δ_u (mm)	Ductility Index (Δ=Δ_u/Δ_y)	Increase in the ductility index %	Failure mode
S0	29	---	22	60	2.73	---	Flexural cracks followed by compression failure
S2	31.9	10	19	60	3.16	15.75	Debonding of the SHCC layer
S2-SC	36	24.1	21	68	3.24	18.68	Debonding of the SHCC layer
R3-SC	45	55.2	27	85	3.15	15.38	Concrete cover splitting
S3	34	17.2	29	80	2.76	1.10	Debonding of the SHCC layer
S3-SC	37	27.6	31	88	2.84	4.03	Debonding of the SHCC layer
R6-SC	42	44.8	33	96	2.91	6.59	Concrete cover splitting

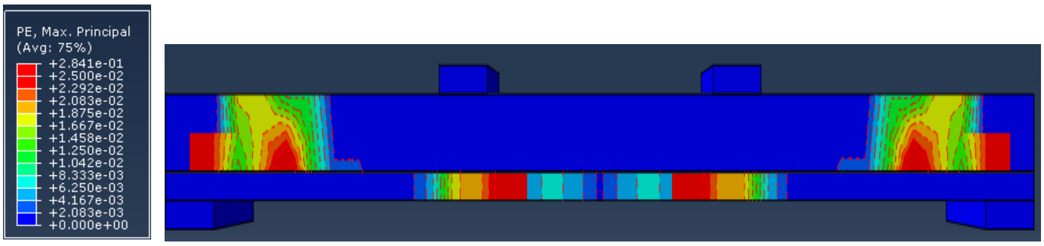

Fig. 29 The numerical failure pattern of the specimen R3-SC

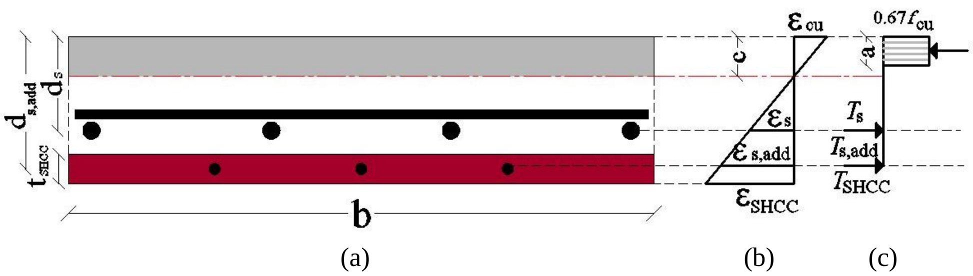

Fig. 30 The analytical model of the SHCC-strengthened RC slabs: (a) cross-section of the strengthened RC slab, (b) strains distribution and (c) equivalent forces

assumptions of the Egyptian code for design and construction of concrete structures, ECP 203-2017. The analysis used internal forces which estimated based on the sectional stress-strain distribution to predict the nominal failure moment as shown in Fig. 30. The suggested assumptions can be summarized as follows:

1. Plane sections before bending remain plane after bending.
2. The tension force developed in the concrete is neglected.
3. An equivalent rectangular stress block may be used to simplify the calculation of the concrete compression force.
4. The tension reinforcement bars had yielded.

Based on the aforementioned assumptions, the nominal failure moment of the slab section was estimated using Eq. (8) while the location of the neutral axis (c) was calculated using Eq. (9).

$$M_n = T_s\ x\ \left(d_s - \frac{a}{2}\right) + T_{s,add}\ x\ \left(d_{s,add} - \frac{a}{2}\right) + T_{SHCC}\ x\ \left(d_{s,add} - \frac{a}{2}\right) \tag{8}$$

$$c = \frac{A_s\ x\ f_y + A_{s,add}\ x\ f_y + f_{t,SHCC}\ x\ A_{SHCC}}{0.8\ x\ 0.67x\ f_{cu}\ x\ b} \tag{9}$$

where T_s is the tensile force developed in the tension reinforcement, $T_{s,add}$ is the tensile force developed in the reinforcement of the SHCC layer, T_{SHCC} is the tensile force of the SHCC layer, C_c is the compressive force developed in the rectangular compressive stress block, d_s is the distance between the slab top soffit and the center of the tension reinforcement, $d_{s,add}$ is the distance between the slab top soffit and the center of the reinforcement embedded in the SHCC layer, t_{SHCC} is the thickness of the SHCC layer, a is the height of the rectangular compressive stress block $= 0.8\,c$, A_s is the area of the tensile reinforcement embedded in concrete, $A_{s,add}$ is the area of the SHCC reinforcement, A_{SHCC} is the area of the SHCC layer, f_y is the yield strength of the tensile reinforcement embedded in concrete, $f_{y,add}$ is the yield strength of the SHCC reinforcement, $f_{t,SHCC}$ is the tensile strength of the SHCC layer, f_{cu} is the compressive strength of concrete, b is the width of the RC slab, ε_{cu} is the ultimate strain of concrete in compression, ε_s is the strain of the tensile reinforcement embedded in concrete, $\varepsilon_{s,add}$ is the strain of the tensile reinforcement of the SHCC and ε_{SHCC} is the strain of the SHCC layer. All parameters required to determine both c and M_n were listed in Table 15. The ultimate failure load (P_u) was estimated simply using the nominal failure moment by applying the principles of structural analysis.

Table 15 Comparison between the experimental and theoretical ultimate failure loads

Beam	Main steel embedded in the concrete layer		Additional steel embedded in the SHCC layer		$f_{t,SHCC}$ (MPa)	A_{SHCC} (mm^2)	c (mm)	a (mm)	d_s (mm)	$d_{s,add}$ (mm)	M_n (kN.m)	$P_{u,theo}$ (kN)	Pu,exp (kN)	$Pu,exp/Pu,theo$
	A_s (mm^2)	f_y (MPa)	$A_{s,add}$ (mm^2)	$f_{y,add}$ (MPa)										
S0	314.16	410	-	-	-	-	19.4	15.5	70	-	8.02	28.28	28	0.99
S1	314.16	410	100.5	245	3.5	8000	27.3	21.8	70	90	9.52	33.59	31	0.92
S2	314.16	410	100.5	245	3.5	12000	29.4	23.5	70	95	10.38	36.62	31	0.85
S3	314.16	410	100.5	245	3.5	16000	31.5	25.2	70	100	11.22	39.57	33	0.83
S4	314.16	410	150.8	245	3.5	8000	29.2	23.3	70	90	10.28	36.26	34	0.94
S5	314.16	410	201	245	3.5	8000	31	24.8	70	90	11.02	38.86	35	0.90
S6	314.16	410	100.5	245	3.5	12000	29.4	23.5	70	95	10.38	36.62	35	0.96

The calculated theoretical failure loads ($P_{u,theo}$) of the tested RC slab specimens combined with the experimental results were listed in Table 15. It was shown that the theoretical model can estimate the ultimate failure loads of the RC slab specimens with acceptable accuracy compared to the experimental results. Ratios between the experimental and the theoretical ultimate failure loads ($P_{u,exp}$ / $P_{u,theo}$) ranged from 0.83 to 0.99.

8. Conclusions

Based on the experimental investigation of the flexural behavior of the RC slabs strengthened with reinforced SHCC layers, the following findings could be drawn:

1. RC slab specimens strengthened using 20 mm of reinforced SHCC layers (S1, S4, and S5) failed under compression failure. Specimen S5 with the largest reinforcement ratio (2.51%) had the highest ultimate failure load equal to 35 kN with increasing ratio of 25% compared to the control RC slab. Despite that, specimen S5 failed under compression failure, it failed with a sufficient ductility index (14.7% higher than the control specimen).
2. As the SHCC layer thickness increased, the failure pattern for the strengthened RC slabs changed from compression failure to SHCC debonding as occurred for specimens S2 and S3 with 30 mm and 40 mm strengthening layer thickness, respectively.
3. Specimen S6 which failed under concrete cover splitting had the highest RC slab cracking load (26.3 kN) and the highest ultimate failure load (25% higher than the control specimen) among all tested specimens. On the other hand, specimen S5 had the highest stiffness while specimen S2 had the highest ductility index.

Additionally, results of the numerical FEM agreed well with the experimental responses for both control and strengthened RC slabs in terms of the ultimate failure load and failure pattern. The cohesive surface model used in the numerical model proved its proficiency to capture the debonding failure mode which is impossible in case of using perfect bond between concrete substrate and SHCC layers. Moreover, the numerical FEM used in a parametric study to show the effect of the reinforcement ratio within the SHCC layer, the thickness of the SHCC layer, and use steel connectors to adjoin the concrete/ SHCC interface on the behavior of the strengthened slabs. Based on the investigated parametric study using the numerical model, the following conclusions could be obtained:

4. The increase of the SHCC reinforcement ratio did not increase remarkably the ultimate failure load of the specimens failed under compression failure. On the contrary, the ultimate failure load and the ductility of specimen S2 which failed due to the debonding of the UHP-SHCC were improved.
5. The failure pattern of the specimen S6 changed from concrete cover splitting to debonding of the SHCC layer by the increase of the SHCC reinforcement ratio causing a significant increase for both the ultimate failure load and the ductility index.
6. Specimens with 10 mm thickness of SHCC layer did not improve the ultimate failure load significantly compared with the control specimen because of the rupture of the strengthening layer. Also, neither the ultimate failure load nor the ductility index significantly improved for the specimens failed under the compression failure mode by the increase of the SHCC layer thickness.
7. For specimens failed by the debonding of the SHCC layer, the increase of the SHCC thickness contributed in the delay of the debonding load. As a result, the ultimate failure load and the ductility index of the specimens T5 and T6 enhanced remarkably compared to specimen S2.
8. As the SHCC layer thickness increased from 30 to 40 mm, the failure pattern converted from concrete cover splitting in specimen S6 to SHCC debonding in specimen T16. As a result, the ultimate failure load for specimen T16 was equal to 55 kN compared to 40 kN in case of specimen S6. Also, the increasing ratio of the ductility index for specimens S6 and T15 compared to the control specimen S0 were 0.73 and 6.96, respectively.
9. The failure pattern changed from debonding of the SHCC layer for specimens S2 and S3 to concrete cover splitting for specimens R3-SC and R6-SC after using connectors of 4D10 spaced every 87.5 mm. The increasing ratio of the ultimate failure load for specimens S2, R3-SC, S3, and R6-SC compared to the control specimen S0 were 10, 55.2, 17.2, and 44.8%, while the increasing ratio of the ductility index were 15.75, 15.38, 1.10, and 6.59%, respectively.

References

Abbaszadeh, M.A., Sharbatdar, M.K. and Kheyroddin, A. (2017), "Performance of two-way RC slabs retrofitted by different configurations of high performance fibre reinforced cementitous composite strips", *Open Civil Eng. J.*, **11**, 650-663. https://doi.org/10.2174/1874149501711010650.

Afefy, H. and El-Tony, M. (2019), "Punching shear resistance of strengthened reinforced concrete interior slab-column connections using ultra-high-performance strain hardening cementitious composite material", *Adv. Struct. Eng.*, **22**(8), 1799-1816. https://doi.org/10.1177/1369433218823841.

Al-Osta, M.A., Isa, M.N., Baluch, M.H. and Rahman, M.K. (2017), "Flexural behavior of reinforced concrete beams strengthened with ultra-high performance fiber reinforced concrete", *Constr. Build. Mater*., **134**, 279-296. https://doi.org/10.1016/j.conbuildmat.2016.12.094.

Basha, A., Fayed, S. and Elsamak, G. (2019), "Flexural behavior of cracked RC beams retrofitted with strain hardening cementitious composites", *KSCE J. Civil Eng.*, **23**(6), 2644-2656. https://doi.org/10.1007/s12205-019-1874-4.

Cheng, M.Y. and Parra-Montesinos, G.J. (2010), "Evaluation of steel fiber reinforcement for punching shear resistance in slab-column connections—part I: monotonically increased load", *ACI Struct. J.*, **107**, 101-109.

Choi, K., Taha, M.R., Park, H. and Maji, A.K. (2007), "Punching shear strength of interior concrete slab-column connections reinforced with steel fibers", *Cement Concrete Compos.*, **29**, 409-420. https://doi.org/10.1016/j.cemconcomp.2006.12.003.

ECP 203-2017 (2017), Design and Construction of Reinforced Concrete Structures.

Esmaeeli, E. (2015), "Development of hybrid composite plate (HCP) for strengthening and repair of RC structures", Doctoral Thesis, University of Minho, Guimaraes, Portugal.

Ganesana, N., Nidhi, M. and Indirac, P.V. (2015), "SFRHPC interior beam-column-slab joints under reverse cyclic loading", *Adv. Concrete Constr.*, **3**(3), 237-250. https://doi.org/10.12989/acc.2015.3.3.237.

Hibbitt, Karlsson, and Sorensen, Inc. (2000), ABAQUS Theory Manual, User Manual and Example Manual, Version 6.7. Providence, RI, Simulia.

Hussein, H., Kunieda, M. and Nakamura, H. (2012), "Strength and ductility of RC beams strengthened with steel-reinforced strain hardening cementitious composites", *Cement Concrete Compos*., **34**(9), 1061-1066. https://doi.org/10.1016/j.cemconcomp.2012.06.004.

Khalil, A., Etman, E., Atta, A. and Essam, M. (2017), "Behavior of RC beams strengthened with strain hardening cementitious composites (SHCC) subjected to monotonic and repeated loads", *Eng. Struct.*, **140**, 151-163. https://doi.org/10.1016/j.engstruct.2017.02.049.

Kunieda, M., Hussein, M., Ueda, N. and Nakamura, H. (2010), "Fracture behavior of steel reinforced UHP-SHCC under axial tension", *Proceedings FRAMCOS-7*, 1557-1564.

Martinola, G., Meda, A., Plizzari, G.A. and Rinaldi, Z. (2010), "Strengthening and repair of RC beams with fiber reinforced concrete", *Cement Concrete Compos*., **32**(9), 731-739. https://doi.org/10.1016/j.cemconcomp.2010.07.001.

Obaidat, Y.T., Heyden, S. and Dahlblom, O. (2010), "The effect of CFRP and CFRP/concrete interface model when modeling retrofitted RC beams with FEM", *Comput. Struct.*, **92**, 1391-1398. https://doi.org/10.1016/j.compstruct.2009.11.008.

Qi, J., Wang, J. and Feng, Y. (2019), "Shear performance of an innovative UHPFRC deck of composite bridge with coarse aggregate", *Adv. Concrete Constr*., **7**(4), 219-229. https://doi.org/10.12989/acc.2019.7.4.219.

Radik, M.J., Erdogmus, E. and Schafer, T. (2011), "Strengthening two-way reinforced concrete floor slabs using polypropylene fiber reinforcement", *J. Mater. Civil Eng*., **23**, 562-571. https://doi.org/10.1061/(ASCE)MT.1943-5533.0000206.

Saenz, LP. (1964), "Discussion of "Equation for the stress-strain curve of concrete", *ACI J*., **61**, 1229-1235.

Sakr, M.A., Sleemah, A.A., Khalifa, T.M. and Mansour, W.N. (2019), "Shear strengthening of RC beams using prefabricated ultra-high performance fiber reinforced concrete (UHPFRC) plates: Experimental and numerical investigation", *Struct. Concrete J.*, **20**, 1137-1153. https://doi.org/10.1002/suco.201800137.

Shin, S.K., Kim, J.J.H. and Lim, Y.M. (2007), "Investigation of the strengthening effect of DFRCC applied to plain concrete beams", *Cement Concrete Compos*., **29**(6), 465-473. https://doi.org/10.1016/j.cemconcomp.2007.02.005.

Yun, H.D., Kim, S.W., Lee, Y.O., Izuka, T., Sakaguchi, Y., Rokugo, K. and Lim, S.C (2010), "Crack width control of reinforced concrete one-way slabs utilizing expansive strain-hardening cement-based composites (SHCCs)", *Proceedings FRAMCOS-7*, 1565-1572.

Zhang, Y. (2013), "Zero-span tensile model for evaluating cracking behavior of SHCC for RC flexural strengthening", *Mag. Concrete Res*., **65**, 1486-1493. https://doi.org/10.1680/macr.13.00215.

JK